December 1987

Two-dimensionat studies of streamers fn gases

S. K. Dhali
Southern Illinois University, Carbondale, Illinois

P. F. Williams
University of Nebraska - Lincoln, pfw@moi.unl.edu

Two-dimensional studies of streamers in gases

S. K. Dhali
Department of Electrical Engineering, Southern Illinois University, Carbondale, Illinois 62901
P. F. Williams
Department of Electrical Engineering, University of Nebraska-Lincoln, Lincoln, Nebraska 68588-0511

(Received 13 April 1987; accepted for publication 13 August 1987)

We present the results of two-dimensional computer simulations of streamer initiation and propagation in atmospheric pressure N_2. The simulation algorithm makes use of flux-corrected transport techniques and was used as a tool to study the solutions of the transport equations under conditions suitable for streamers, for which realistic analytic solutions are not known. We present and discuss conclusions about streamer transport based on the results of these studies. Finally, we present a novel method of checking on the numerical accuracy with which the algorithm solves the transport equations.

I. INTRODUCTION

Since the streamer mechanism was first suggested by Raether,[1] and Loeb and Meek,[2] a sizable volume of evidence has accumulated showing the importance of streamers or fast ionizing waves to several aspects of electrical breakdown of gases. Many reports of studies of streamer behavior have appeared. Theoretical efforts have been hampered by the fact that the mathematical description of transport under conditions appropriate for streamers proves difficult to deal with in general. There are two principal difficulties. First, the problem is inherently two dimensional (at least), and attempts to make use of one-dimensional approximations have limited validity. Second, in numerical approaches to the problem, difficulties are generally encountered because of the very steep, shocklike, density gradients that appear. Most numerical algorithms for integrating the relevant continuity equations experience difficulty in dealing with these steep gradients. Consequently, quantitative understanding of streamers in gases is limited. The characteristics of the streamerlike solutions of even the simplest set of equations containing the basic streamer physics are unknown.

We describe the results of numerical calculations of streamer propagation based on a fully two-dimensional algorithm which makes use of flux-corrected transport techniques to handle the steep density gradients. Development of the algorithm has allowed us to investigate problems in streamer propagation of considerable interest that have not been accessible to previous workers. In this paper we describe the algorithm in some detail, and we present results of the application of the algorithm to questions of the dependence of streamer propagation on ionization ahead of the streamer, on applied field, and on initial conditions.

We take a somewhat different approach from previous workers in the field. Our ultimate aim, as was theirs, is to understand at a quantitative level streamer propagation under realistic conditions. However, we recognize that the present state of knowledge in the area falls far short of this goal. A simple set of partial differential equations may be constructed that contains the basic physics of streamer formation and propagation, but may ignore or inadequately describe one or more mechanisms important to the evolution of streamer under realistic conditions. However, the characteristics of the solutions of even this minimal set are known only in the most superficial terms. Basic properties of these solutions such as propagation velocity, diameter, and ionization density inside the streamer, or the dependence of these properties on environmental conditions are not known.

Accordingly, our goal in this work has been to use the numerical results as a tool to aid us in determining and understanding the characteristics of these solutions. Therefore, we do not attempt to match specific experimental results. Instead, after ensuring that our numerical algorithm is solving the differential equations accurately, we make use of it to determine these solutions and to ask what the effect of specific changes in environment on these solutions are. We leave for later study such questions as the details of the photoionization mechanism and the importance of nonequilibrium processes at the streamer tip.

II. SCIENTIFIC BACKGROUND

The streamer mechanism was first proposed by Raether[1] and Loeb and Meek[2] to explain the electrical breakdown of strongly overvolted spark gaps at near-atmospheric pressure. They suggested that when the electron avalanche grows to a size such that it is capable of partially shielding itself from the applied field (estimated to occur when the avalanche size reaches about 10^8 electrons) the propagation and growth of the avalanche change markedly. Specifically, the charges that appear on the surface of the streamer plasma to shield the interior unavoidably enhance the electric field over a limited region just outside the streamer. The degree of enhancement depends on the degree of shielding and on the geometry of the streamer, ranging for perfect shielding from a factor of 2 for a planar front, to 3 for a spherical front, to very large values for sharp, needlelike shapes. For fields near that required for breakdown, the Townsend ionization coefficient α is a strong function of electric field, so that even modest field enhancements can result in substantial increases in ionization rate. If a mechanism such as transport or photoionization exists that places a few free seed electrons just in front of the streamer head, avalanching in the locally enhanced field can cause the streamer to propagate with velocities much larger than the peak electron drift velocity. Additionally, the ionization

 0021-8979/87/244696-12$02.40

density in the streamer body can build up to values considerably larger than that necessary to initiate streamer formation.

The simplest set of equations containing the basic physics necessary for streamer formation and propagation are the continuity equations for electrons and positive ions coupled with Poisson's equation for the electric field, along with various constitutive relations for the drift velocities, ionization coefficient, etc.[3]

$$\frac{\partial n_e}{dt} + \nabla\cdot(\mathbf{v}_e n_e) - D_e \nabla^2 n_e = \alpha n_e v_e + S, \tag{1a}$$

$$\frac{\partial n_+}{dt} + \nabla\cdot(\mathbf{v}_+ n_+) - D_+ \nabla^2 n_+ = \alpha n_e v_e + S, \tag{1b}$$

$$\nabla^2 \Phi = -q_e(n_+ - n_e)/\epsilon_0, \tag{2}$$

where n_e, $\mathbf{v}_e$, D_e, n_+, $\mathbf{v}_+$, and D_+ are the particle density, velocity, and diffusivity for the electrons and positive ions, respectively, v_e is the magnitude of $\mathbf{v}_e$, α is the Townsend ionization coefficient, Φ is the electric potential, q_e is the (unsigned) electronic charge, and ϵ_0 is the permittivity of free space. The term S may describe effects of any of several particle source or sink mechanisms such as photoionization or recombination. In an attaching gas, a third continuity equation for negative ion species would be needed and a distinct S term would be required in each equation. The charge density in the right-hand side of Eq. (2) would also be modified to include the negative ion density.

Several attempts at the analtyic solution of these equations have been reported.[4–8] Most have been essentially one dimensional and have made use of questionable approximations for dealing with the electric field. The evident difficulties associated with solving the relevant transport equations analytically led many workers to consider a numerical solution. In the early work, the problem was generally treated one dimensionally, resulting in serous limitations on the applicability of the results because of the substantial errors introduced into the calculations of electric field strength by the one-dimensional approximation. Davies, Davies, and Evans reported a numerical algorithm that is basically one dimensional, but treats the electric field in an approximately correct two-dimensional way.[9] However, assumptions must be made about the radial profile of the streamer which preclude studies of the evolution of the shape of the streamer tip. The algorithm was extended to allow fully two-dimensional calculations, but the authors reported stability problems because of the numerical derivatives involved.[10]

The algorithm described by Davies and co-workers was based on the use of the method of characteristics to integrate the continuity equations. Several workers adopted the technique. Kline reported the results of similar, one-dimensional calculations that included photoionization as well as photoemission effects.[11] Yoshida and Tagashira[12] reported calculations similar to those of Davies, Evans, and Woodison,[13] except that they included photoionization effects, and took into account the effects of molecular excitation on secondary ionization processes. Yoshida and Tagashira[14] have also reported a two-dimensional calculation similar to that of Davies *et al.*[10]

Marode has described a different approach, in which the dependence of the electric field on the charge density was handled by modeling the streamer filament as a distributed capacitance.[15] The one-dimensional continuity equation for electron density was then solved numerically using a finite difference technique. Abbas and Bayle[16] have used a numerical algorithm similar to that of Davies *et al.*[10] to examine the structure of the streamer wavefront, and to study the dependence of this structure on the electron density in front of the streamer. More recently, these authors have suggested that effects resulting from energy transport in regions of large temperature gradients may not be negligible in a propagating streamer.[17]

The algorithm we describe obviates the two principal difficulties encountered by previous workers attempting numerical simulation of streamer transport: it is well suited to handling the very steep density gradients that appear at the head of a propagating streamer, and it is fully two dimensional. The algorithm uses two-dimensional flux-corrected transport techniques which allow us to solve numerically the transport equations under strongly space-charge-dominated conditions such as occur at the head of a propagating streamer, to follow the radial development of the streamer, and to include effects of nonuniform distribution of secondary electrons resulting from photoionization or photoemission from the cathode. The algorithm has proven stable and capable of dealing with the steep density gradients that appear in these calculations. To our knowledge, this work represents the first systematic application of this technique to the problem of space-charge-dominated transport in a fully two-dimensional model.

III. THE MODEL

We assume the electrons and positive ion densities to be governed by Eqs. (1) and (2) where the drift velocities and impact ionization coefficient α, are unique, empirically determined functions of E/P. We include diffusion, identifying both transverse and longitudinal diffusion components, and choose values for these parameters appropriate for N_2 at 760 Torr. Specifically, for pressure P, in Torr, and electric field E, in V/cm, we used[9]

$$\alpha = 5.7Pe^{-260P/E} \quad (\mathrm{cm}^{-1}).$$

For the fields of interest, the electric field dependence of the electron and ion drift velocities are well approximated by a simple constant mobility model,[9]

$$\mu_e = 2.9\times 10^5/P \quad (\mathrm{cm}^2/\mathrm{V\,s})$$

$$\mu_p = 2.6\times 10^3/P \quad (\mathrm{cm}^2/\mathrm{V\,s}).$$

The transverse and logitudinal diffusion coefficients, D_L and D_T, are taken as $D_L = 1800$ and $D_T = 2190$ cm^2/s.[1,18] We neglect positive ion diffusion.

In our calculations, we were primarily interested in studying the dependence of streamer propagation on the free ionization density ahead of the streamer. Accordingly, for the calculations presented here we have not included photoionization in the source term S in Eqs. (1). Instead, we have simulated photoionization by including, as an initial condition, a tenuous neutral ionization of density 10^5–10^8

cm^{-3} uniformly deposited throughout the gap. This approach has the advantage that it allows the direct study of the dependence of streamer propagation on the ionization density ahead of it.

The external circuit consists of a resistor R in series with a gap of length d. If $V_g(t)$ represents the voltage on the discharge and V the externally applied voltage, then

$$V_g = V - RI_g(t), \tag{3}$$

where

$$I_g(t) = \frac{q_e}{d}\int_{\text{gap}} (n_+ \mathbf{v}_+ - n_e \mathbf{v}_e)\cdot\hat{e}_z \, d^3r, \tag{4}$$

$\hat{e}_z$ being a unit vector in the z direction, and the integral being taken over the volume of the gap. V_g is calculated at each time step and then used as a bounary condition at the charged electrode for Eq. (2) for the next step. For our simulations, we took $R = 50\ \Omega$, and the gap was assumed to be plane parallel with a 5-mm electrode separation. The breakdown voltage determined experimentally for such a gap at 760 Torr was found to be 17.7 kV.

In order that a streamer form immediately, in all the calculations reported here we placed, as an initial condition, a spheroid or hemispheroid of relatively dense plasma (10^{13}–10^{15} cm^{-3}) either in gap center or on an electrode. The spheroids had a Gaussian shape in both the radial and axial directions. We discuss in a later section the dependence of the propagating streamer on parameters describing the spheroids.

IV. NUMERICAL METHOD

Equations (1) can be numerically integrated using a finite-difference technique. The accuracy of the method depends on the order of the difference scheme. Higher-order (second and above) schemes produce ripples near steep gradients. First-order schemes such as donor cell do not produce ripples, but suffer from excessive numerical diffusion. Flux-corrected transport constructs the net transportive flux point-by-point as a weighted average of a flux computed by a first-order scheme and a flux computed by a high-order scheme. The weighting is done so that the high-order flux is used to the greatest extent possible without introducing false ripples.[19]

Flux-corrected transport techniques were developed by Boris and Book to model one-dimensional shock fronts in fluids.[20] Zalesak extended the one-dimensional method to a multidimensional flux corrector for fluid problems,[19] and Morrow has used the one-dimensional method to study problems related to space charge in partially ionized gases.[21] Fernsler has reported the use of a modified SHASTA FCT algorithm to implement two-dimensional streamer simulations, but the work was not pursued.[22] Recently, Wu and Kunhardt have described a modification of the FCT algorithm in which essentially the logarithm of the species density is followed.[23] Our algorithm extends the multidimensional work of Zalesak to be applicable to axially symmetric, space-charge-dominated transport problems such as encountered in modeling streamers.

From Eqs. (1), the convective contribution to the density derivative is

$$\left.\frac{\partial N}{\partial t}\right|_{\text{conv}} = -\nabla\cdot(N\mathbf{v}), \tag{5}$$

where N is the density of the relevant species and $\mathbf{v}$ is the drift velocity. Treating (rN) as the dependent variable, we have for axially symmetric geometry

$$\left.\frac{\partial (rN)}{\partial t}\right|_{\text{conv}} = -\frac{\partial f}{\partial r} - \frac{\partial g}{\partial z}, \tag{6}$$

where $f = rNv_r$, $g = rNv_z$, and $\mathbf{v} = v_r\hat{e}_r + v_z\hat{e}_z$.

We use the modified Euler difference approximation[24] to Eq. (6) to implement the time integration in the high-order case, and a simple Euler approximation for the low order. We divide two-dimensional space into a grid of points and denote, for example, the density at the ith radial and jth axial point by $N_{i,j}$. We assume that at the beginning of a time step values of $N_{i,j}$, $f_{i,j}$, and $g_{i,j}$ are known at all grid points at time t. The modified Euler finite-difference approximation to Eq. (6) in flux form that we used for the high-order calculation is

$$N_{i,j}^{t+\Delta T/2} = N_{i,j}^{t} - \frac{\Delta T}{2r_{i,j}V_{i,j}}\left(F_{i+\frac{1}{2},j}^{t} - F_{i-\frac{1}{2},j}^{t} + G_{i,j+\frac{1}{2}}^{t} - G_{i,j-\frac{1}{2}}^{t}\right), \tag{7a}$$

$$N_{i,j}^{t+\Delta T} = N_{i,j}^{t} - \frac{\Delta T}{r_{i,j}V_{i,j}}\left(F_{i+\frac{1}{2},j}^{t+\Delta T/2} - F_{i-\frac{1}{2},j}^{t+\Delta T/2} + G_{i,j+\frac{1}{2}}^{t+\Delta T/2} - G_{i,j-\frac{1}{2}}^{t+\Delta T/2}\right), \tag{7b}$$

where $V_{i,j}$ and $r_{i,j}$ are the volume and radius of the i,jth cell, and F^t and G^t are the fluxes corresponding to $f = rNv_r$ and $g = rNv_z$, respectively, at time t.

The functional forms of F^t and G^t are determined by the order of the difference scheme. Following Zalesak,[19] and assuming an equally spaced mesh in the z direction, the eighth-order fluxes are

$$F_{i+\frac{1}{2},j} = \pi\Delta z(r_{i,j} + r_{i+1,j})\left(\frac{533}{840}(f_{i+1,j} + f_{i,j}) - \frac{139}{840}(f_{i+2,j} + f_{i-1,j}) + \frac{29}{840}(f_{i+3,j} + f_{i-2,j}) - \frac{1}{280}(f_{i+4,j} + f_{i-3,j})\right), \tag{8a}$$

$$G_{i,j+\frac{1}{2}} = \frac{\pi(r_{i-1,j} + 2r_{i,j} + r_{i+1,j})(r_{i+1,j} - r_{i-1,j})}{4}\times\left(\frac{533}{840}(g_{i,j+1} + g_{i,j}) - \frac{139}{840}(g_{i,j+2} + g_{i,j-1}) + \frac{29}{840}(g_{i,j+3} + g_{i,j-2}) - \frac{1}{280}(g_{i,j+4} + g_{i,j-3})\right). \tag{8b}$$

The first-order calculation of the convective contribu-

tion was handled using a donor cell algorithm with simple Eulerian time integration

$$N_{i,j}^{t+\Delta T} = N_{i,j}^{t} - \frac{\Delta T}{V_{i,j}} (F_{i+\frac{1}{2},j}^{t} - F_{i-\frac{1}{2},j}^{t} + G_{i,j+\frac{1}{2}}^{t} - G_{i,j-\frac{1}{2}}^{t}) . \quad (9)$$

The donor cell fluxes are

$$F_{i+\frac{1}{2},j} = \pi \Delta z (r_{i,j} + r_{i+1,j})(\tilde{v}_r)_{i+\frac{1}{2},j} \times \begin{bmatrix} N_{i,j} & \text{if } (\tilde{v}_r)_{i+\frac{1}{2},j} \geq 0 \\ N_{i+1,j} & \text{if } (\tilde{v}_r)_{i+\frac{1}{2},j} < 0 \end{bmatrix}, \quad (10a)$$

$$G_{i,j+\frac{1}{2}} = \frac{\pi (r_{i-1,j} + 2r_{i,j} + r_{i+1,j})(r_{i+1,j} - r_{i-1,j})}{4} \times (\tilde{v}_z)_{i,j+\frac{1}{2}} \begin{bmatrix} N_{i,j} & \text{if } (\tilde{v}_z)_{i,j+\frac{1}{2},j} \geq 0 \\ N_{i,j+1} & \text{if } (\tilde{v}_z)_{i,j+\frac{1}{2},j} < 0 \end{bmatrix}, \quad (10b)$$

where

$$(\tilde{v}_r)_{i+\frac{1}{2},j} = [(v_r)_{i,j} + (v_r)_{i+1,j}]/2$$

and

$$(\tilde{v}_z)_{i,j+\frac{1}{2}} = [(v_z)_{i,j} + (v_z)_{i,j+1}]/2.$$

The contributions from the diffusion terms and from the impact ionization term in Eqs. (1) were calculated at each time step and added to the convective term $\partial N/\partial t]_{\text{conv}}$. The diffusion term is given by

$$\left.\frac{\partial N}{\partial t}\right|_{\text{diff}} = D_L (N_{i,j+1}^{t} + N_{i,j-1}^{t} - 2N_{i,j}^{t}/\Delta z^2 + \pi D_T \left(\frac{r_{i+1} + r_i}{r_{i+1} - r_i} (N_{i+1,j}^{t} - N_{i,j}^{t}) - \frac{r_i + r_{i-1}}{r_i - r_{i-1}} (N_{i,j}^{t} - N_{i-1,j}^{t}) \right) \frac{\Delta z}{V_{i,j}} . \quad (11)$$

Because of the importance and the rapid variation of the impact ionization term, a second-order scheme was used to calculate it:

$$\Delta N_{i,j}^{\Delta T/2} = \frac{\Delta T}{2} \alpha |v_e| N_{i,j}^{t}, \quad (12a)$$

$$N_{i,j}^{t+\Delta T/2} = \frac{N_{i,j}^{t} + N_{i,j}^{t+\Delta T}}{2} + \Delta N_{i,j}^{\Delta T/2}, \quad (12b)$$

$$\left.\frac{\partial N}{\partial t}\right|_{\text{ionize}} = \alpha |v_e| N_{i,j}^{t+\Delta T/2} . \quad (12c)$$

The electric field was determined by solving Poisson's equation

$$\nabla^2 \Phi = -\rho/\epsilon_0 \quad (13)$$

for the potential function $\Phi(r,z)$, in terms of the driving function $\rho(r,z)$ in the cylindrical domain $0<z<d$ and $0<r<R$, where d is the gap spacing, and R is a suitably chosen large number. The boundary conditions on Φ are $\Phi(r,0) = 0$, $\Phi(r,d) = V$,

$$\left.\frac{\partial \Phi}{\partial r}\right|_{r=0} = 0,$$

and $\Phi(R,z) = Vz/d$. We used the algorithm developed by Kunhardt and Williams to solve Eq. (13).[25] The algorithm is based on using a fast Fourier transform in the z direction and a cubic spline interpolation in the r direction. The algorithm has proven reasonably fast and capable of dealing with the rapidly changing charge densities encountered in streamer calculations.

V. RESULTS

In all simulations described here the initial charge has a Gaussian shape with peak density 10^{14} cm^{-3}, and $1/e$ radii of 0.27 and 0.21 mm in the z and r directions, respectively. A uniform, neutral ionization density of 10^8 cm^{-3} was placed in the gap as an initial condition. Transport parameters were chosen to be those appropriate for 760 Torr of N_2. The gap was taken to have 5-mm separation. For most of the calculations we present here, the applied voltage was 26 kV, giving a field of 52 kV/cm (193 Td at this pressure) and corresponding to about 47% overvoltage.

A. Basic properties

If the initial charge was placed on the anode, a well-defined cathode-directed streamer was formed. Figures 1(a) and 1(b) show the time evolution of the on-axis electron density and the axial electric field component, respectively, for a cathode-directed streamer. Placing the initial charge on the cathode, on the other hand, produced a well-defined anode-directed streamer, and Fig. 2 shows corresponding electron density and field for this case.

Several observations can be made from these data. After an initial period of adjustment, the streamer propagates in a nearly steady-state mode. The velocity of propagation is in the $0.5–2\times10^8$ cm/s range for the cathode-directed streamer, and $1–2\times10^8$ cm/s for the anode-directed streamer. The electron density just behind the streamer head is roughly constant, decreasing slowly as the streamer propagates, and is about 10^{14} cm^{-3}. The electron density behind the cathode-directed streamer tip is a little larger than the density behind the anode-directed tip.

Substantial electric field enhancement is observed in front of the streamer tip. For these conditions, the maximum value of the field was about 3.0 and 2.3 times the applied field intensity in front of the cathode- and anode-directed streamers, respectively. The field inside the streamer body is not completely shielded. Particularly at later times, when the streamer has traversed more than half of the gap, there is considerable field penetration, and electron impact ionization occurs inside the streamer body, raising the free ionization density.

Field penetration occurs because of the finite dielectric relaxation time of the streamer plasma. We estimate the dielectric relaxation time of the plasma by $\tau_D = \epsilon_0/\sigma = \epsilon_0/q_e \tilde{n}_e \mu_e$, where σ is some average conductivity and $\tilde{n}_e$ is some average electron density in the streamer sheath.[26] Inside the streamer and on-axis, the quantity n_e

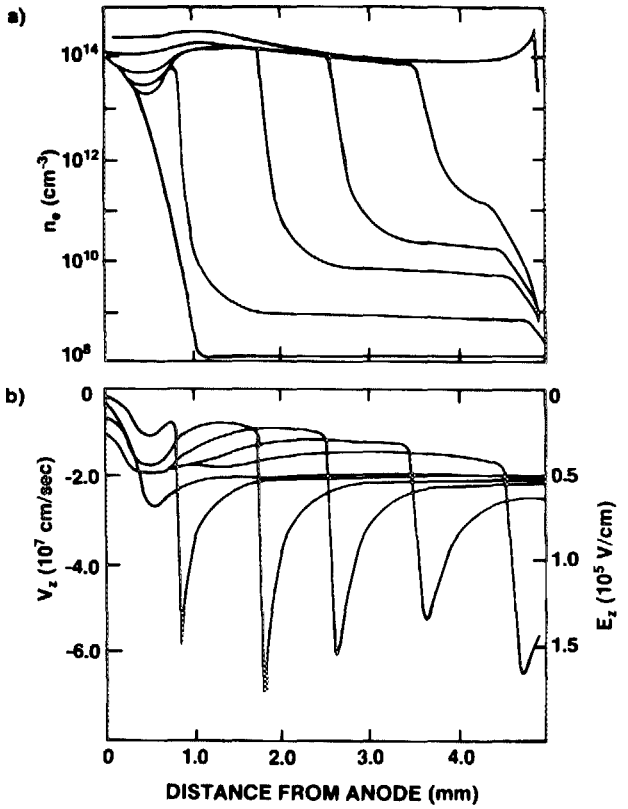

FIG. 1. Plots showing (a) on-axis electron density and (b) electric field and drift velocity for a cathode-directed streamer. The curves correspond to times of $t = 0.1$, 1.0, 2.0, 2.5, 3.0, and 3.5 ns after the start of the simulation. The gap spacing was 0.5 cm, the applied voltage was 26 kV, and the fill gas was pure N_2 at 760 Torr, making the gap about 47% over-volted. The initial ionization distribution was a hemispheroid placed on the anode with a Gaussian density distribution in both radial and axial directions. The peak density was 10^{14} cm^{-3}, and the $1/e$ radii were 0.27 and 0.21 mm in the axial and radial directions, respectively. A uniform, neutral ionization density of 10^8 was placed in the gap as an initial condition.

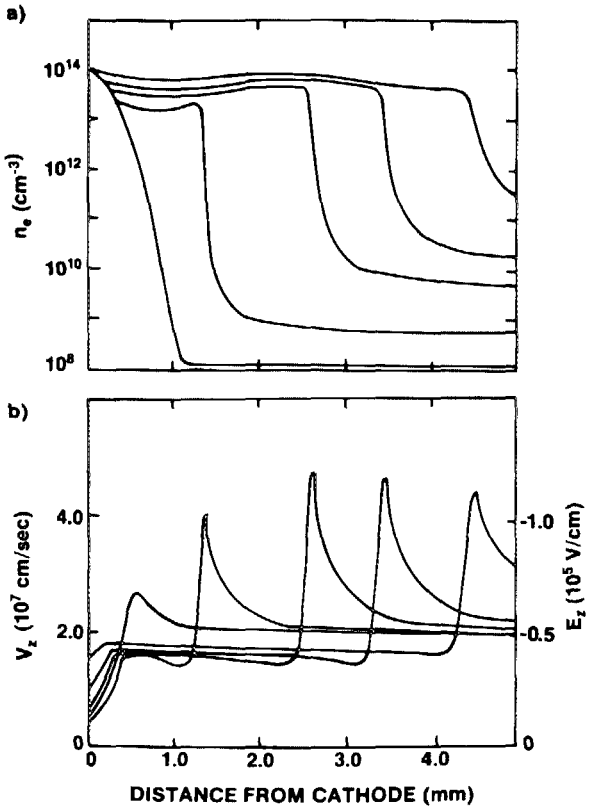

FIG. 2. Plots showing (a) on-axis electron density and (b) electric field and drift velocity for an anode-directed streamer for $t = 0.1$, 1.0, 2.0, 2.5, and 3.0 ns after the start of the simulation. All other conditions were the same as for Fig. 1.

varies from 1.5×10^{14} to 2×10^{13} cm^{-3}, placing τ_D in the range $10 < \tau_D < 72$ ps. The thickness of the charge sheath at the streamer front is $\approx$0.05 mm. At a speed of 1.5×10^8 cm/s, this distance is traversed in 33 ps. Thus, the dielectric relaxation time is comparable to the time scale in which the charge density changes.

Shielding of the streamer interior requires the transport of net charge to the moving head. Thus, an electric field is required inside the streamer body. The magnitude of the field is determined by the streamer conductivity and by the required current flow. Assuming a mean electron density of 10^{14} cm^{-3}, the conductivity of the plasma in the streamer body is 6×10^{-3} $(\Omega\,\text{cm})^{-1}$. If the shielding is only 50% effective, the field inside the streamer from the condition in Figs. 1 and 2 is about 26 kV/cm, and $J \approx 160$ amp/cm^2.

In both Figs. 1 and 2 the background ionization density well ahead of the streamer clearly increases with time. This effect is due to avalanche multiplication in the applied field, as demonstrated by calculations carried out with lower applied fields which show the effect substantially reduced. The slow changes in streamer properties (speed, density gradient at the head, and remnant ionization density in the streamer body) after the initial period of adjustment are partly caused by the changing background ionization into which the streamer propagates. This conclusion is supported by the results of calculations we have carried out in which the Townsend ionization coefficient α, was taken to have an artificial cutoff. Here α was zero for fields below a threshold value, taken to be about 10% greater than the applied field, but had the normal value for larger fields. As expected, the ionization density well ahead of the streamer remained constant, and the changes in time of the streamer properties were reduced in these calculations. However, even in this case a true steady-state propagation condition was not reached.

The spatial development of streamers of both polarities is similar. Figures 3(a)–3(c) and 3(d)–3(f) show contour plots of the electron density and axial electric field in a cathode-directed streamer for three different times. The conditions are the same as for Fig. 1. Similar plots for an anode-directed streamer are shown in Fig. 4. For streamers of both polarities, the streamer diameter as defined by the half-density points stays roughly constant with time, although for the cathode-directed streamer the diameter of the more tenuous outer layers increases slowly.

The gap current can be calculated from Eq. (4). The results are similar for streamers of both polarities and Fig. 5 shows the gap current for the cathode-directed streamer depicted in Figs. 1 and 3, and for the anode-directed streamer in Figs. 2 and 4. The initial current results from the initial ionization distribution shielding itself from the applied field.

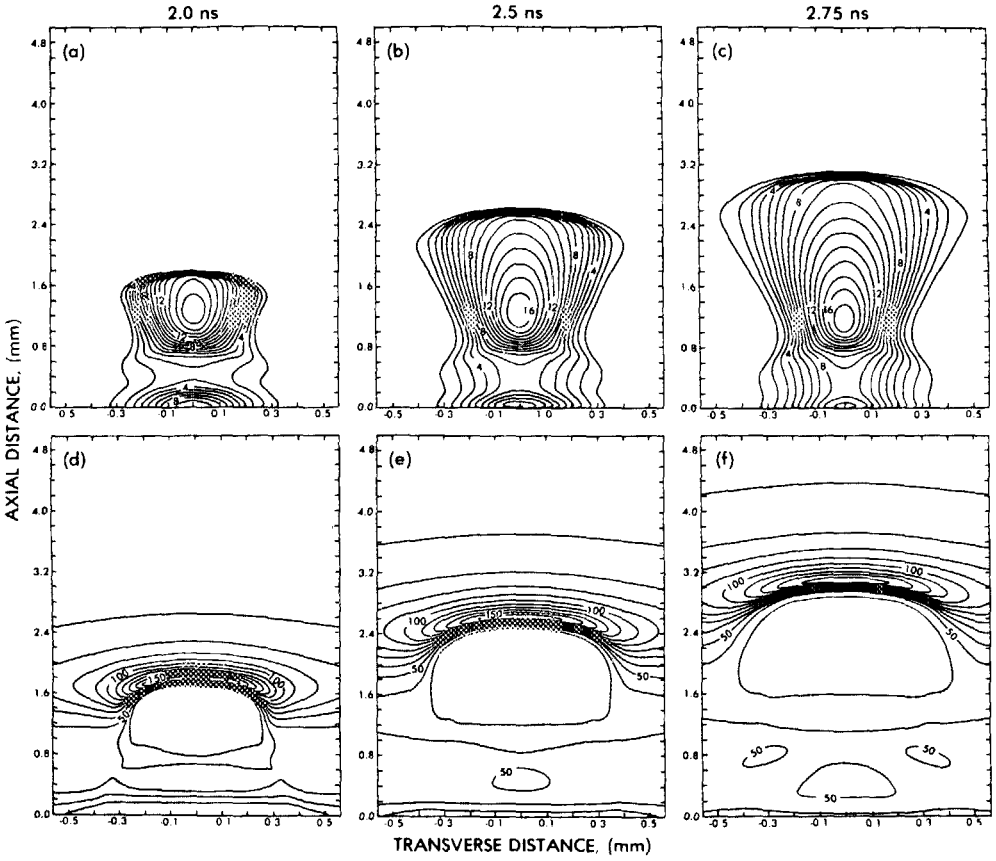

FIG. 3. Contour plots showing the two-dimensional free-electron density [plots (a)–(c)] and axial electric field [plots (d)–(f)] for a cathode-directed streamer at (a) 2.0, (b) 2.5, and (c) 2.75 ns after the start of the simulation with an applied voltage of 26 kV (193 Td). All other conditions were the same as in Fig. 1. For the electron density plots the contour spacing is 1×10^{13} cm^{-3} and the contour labels are scaled by 10^{13} cm^{-3}. For the electric field plots the contour spacing is 10 kV/cm and the contour labels are scaled by 1 kV/cm.

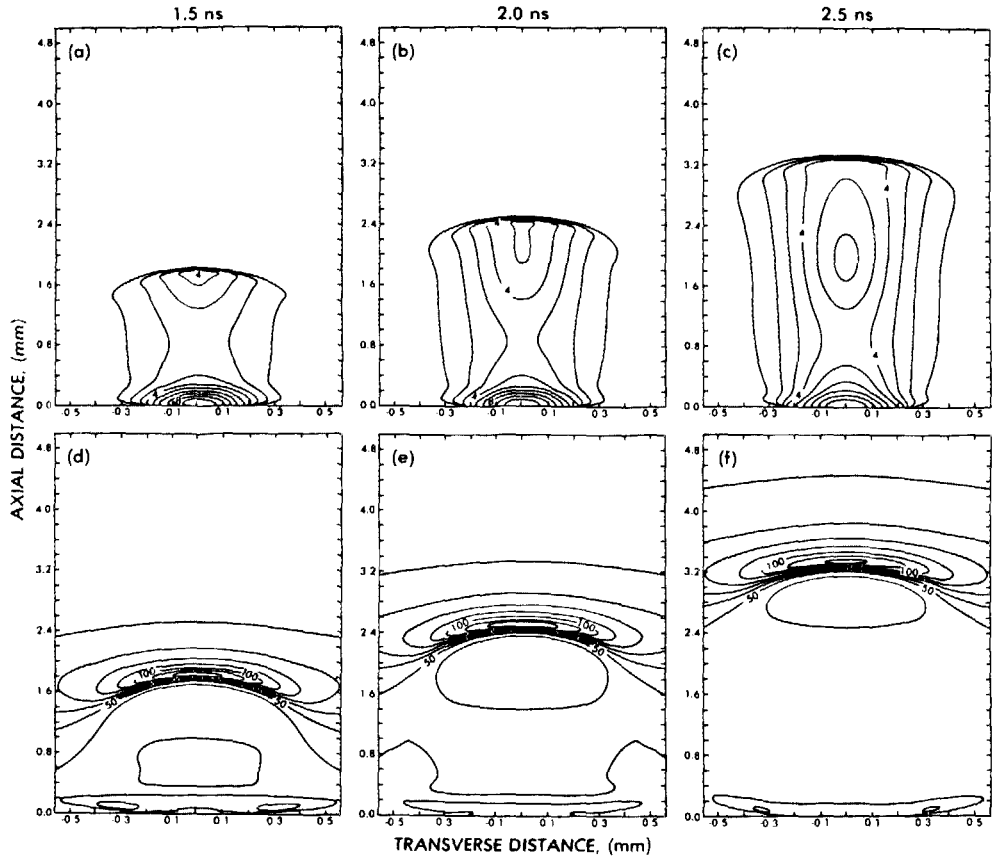

FIG. 4. Contour plots showing the two-dimensional free-electron density [plots (a)–(c)] and axial electric field [plots (d)–(f)] for an anode-directed streamer at (1) 1.5, (b) 2.0, and (c) 2.5 ns after the start of the simulation with an applied voltage of 26 kV (193 Td). All other conditions were the same as in Fig. 2. For the electron density plots the contour spacing is 1×10^{13} cm^{-3} and the contour labels are scaled by 10^{13} cm^{-3}. For the electric field plots the contour spacing is 10 kV/cm and the contour labels are scaled by 1 kV/cm.

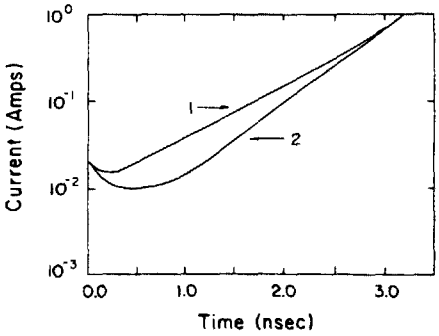

FIG. 5. Gap current as a function of time for (a) anode-directed and (b) cathode-directed streamers. All conditions are the same as in Figs. 1 and 2.

The later, nearly exponential rise is due primarily to the avalanche multiplication of ionization density inside the body of the streamer. These results, combined with the radial distribution of free-electron density given in Figs. 3 and 4 are in good agreement with our earlier estimate of $J \approx 160$ Amp/cm^2 in the streamer body.

If it is accepted that in Figs. 1–4 the densities and fields rapidly reach a quasi-steady-state value determined primarily by the ionization density ahead of the streamer, then we may make use of these data to determine the dependence of various streamer parameters on the ionization density. In Fig. 6 we show plots of the streamer velocity versus the ionization density ahead of the streamer for three applied voltages and for both polarities for calculations in which the initial preionization density was 10^8 cm^{-3}. After an initial start-up transient, the velocity of the cathode-directed streamer seems to depend primarily on the electron density ahead of the streamer, with only a weak dependence on applied field. For the anode-directed streamer, a stronger dependence on applied field is found, but the ionization density ahead of the streamer is still an important parameter.

However, further calculations show that this dependence is actually more complex. In Fig. 7 we show similar data to Fig. 6 for a fixed applied voltage of 30 kV (233 Td), but for two different initial preionization densities of 10^6 and 10^8 cm^{-3}, respectively. These results show that for a fixed voltage the streamer velocity is not a unique function of preionization density ahead of the streamer, and that other parameters must exert a strong influence over the streamer velocity. Particularly for the anode-directed streamer, the time since streamer initiation appears to be the controlling parameter. Close examination of the electron density data in Figs. 1 and 2 shows that the length of the "foot" at the tip of the streamer increases with time, effectively increasing the ionization density that the main, steep, part of the tip sees.

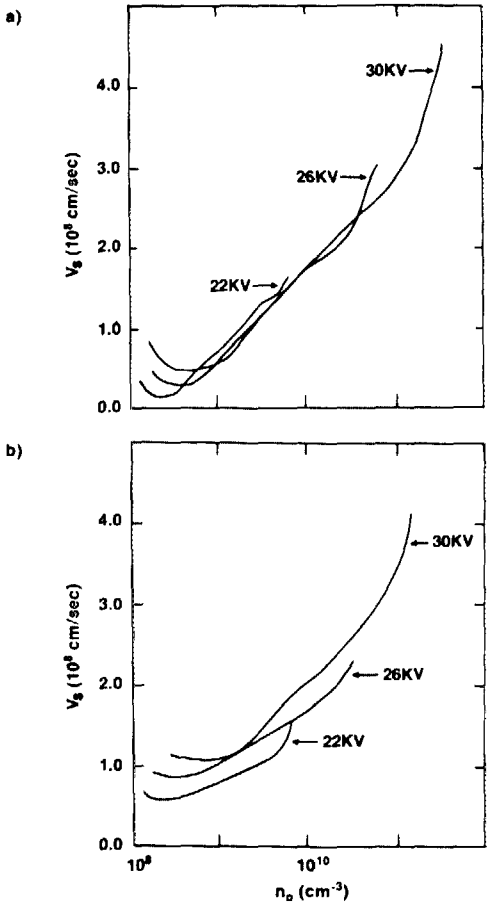

FIG. 6. Streamer velocity vs free-electron density in front of the streamer for (a) cathode-directed and (b) anode-directed streamers for charging voltages of 22 (164 Td), 26 (193 Td), and 30 (223 Td) kV, corresponding to overvoltages of 24%, 47%, and 70%. All other conditions were the same as in Figs. 1 and 2.

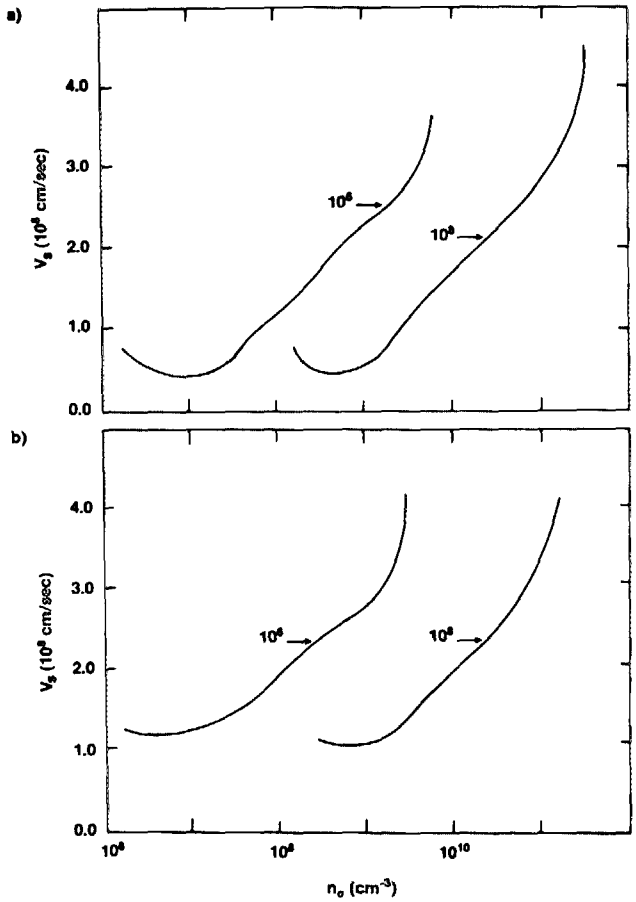

FIG. 7. Streamer velocity vs free-electron density in front of the streamer for (a) cathode-directed and (b) anode-directed streamers for 30 kV (223 Td) charging voltage, and for initial preionization densities of 10^6 and 10^8 cm^{-3}. All other conditions were the same as in Figs. 1 and 2.

The fundamental difference between the cathode- and the anode-directed streamer is the direction of electron drift relative to the streamer propagation. The anode-directed streamer can propagate without any means of producing secondary electrons in front of it because the electron drift provides the necessary electrons, but the cathode-directed streamer cannot. This point is illustrated by a set of calculations we carried out in which neither photoionization nor preionization was included. In the anode-directed case the streamer was able to propagate out of the Gaussian tail of the initial ionization distribution, although the density gradient at the head became quite steep and eventually led to a numerically instability. However, in the cathode-directed case the streamer came to a halt as it encountered the tenuous outer edges of the initiating ionization distribution. Under these conditions the streamer became very narrow, with a sharp tip which produced large field enhancements just ahead of it. The extreme density gradients soon led to a strong numerical instability.

At some point, the cathode-directed streamer should be able to propagate by means of the electron transported by diffusion. Our numerical algorithm would require a finer axial mesh spacing then we used to handle the extreme density gradients required, and we were not able to follow the evolution to this point. In any case, nonequilibrium processes would probably become important and our model would have to be modified.

B. Effects of initial conditions

To determine the effect of the initial ionization conditions on streamer propagation, we carried out several calculations in which differing initial conditions were assumed. To determine the effect of the initial distribution, we made calculations in which the peak density in the initial ionization hemispheroid varied between 10^{13} and 10^{15} cm^{-3}, but all other parameters were fixed. The results for a cathode-directed streamer for initial densities of 10^{13}, 10^{14},and 10^{15} cm^{-3} are shown in Fig. 8. Although the formation of the streamer was more rapid with the higher initial densities because of the reduced dielectric relaxation time of the plasma, after steady state had been reached the properties of the streamers in the three cases were essentially the same. The small differences observed are probably due primarily to avalanching of the uniform background ionization in the applied field. Similar results were observed for anode-directed streamers, leading us to conclude that the properties of the streamer, once formed, are not strongly dependent on the initiating ionization density.

To determine the effect on the streamer of the shape of the initial ionization distribution, we carried out calculations with differing diameters of the Gaussian distribution, but with all other parameters held fixed. Figure 9 shows the

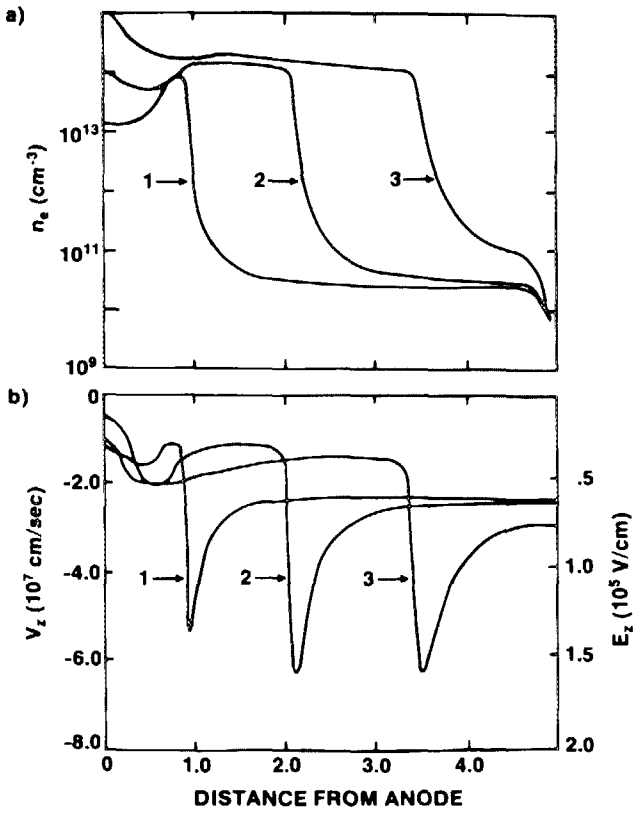

FIG. 8. Plots of (a) electron density and (b) axial electric field for cathode-directed streamers at $t = 1.5$ ns after the start of the simulation. The applied voltage was 30 kV (223 Td), and all conditions were the same as in Fig. 1, except that the ionization density in the initial hemispheroid was (1) 10^{13}, (2) 10^{14}, and (3) 10^{15} cm^{-3}.

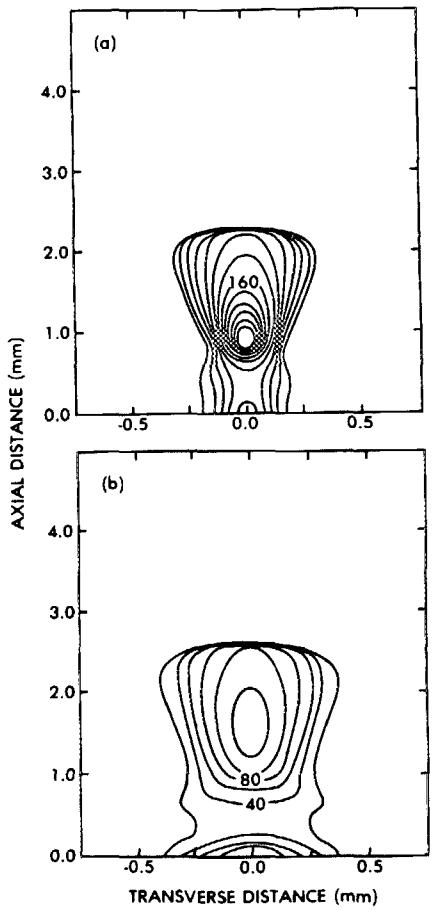

FIG. 9. Contour plots of the two-dimensional electron density for cathode-directed streamers at $t = 2.5$ ns after the start of the simulation. All conditions were the same as in Fig. 1, except that $1/e$ diameter in the radial direction of the initial plasma hemispheroid was (a) 0.28 and (b) 0.58 mm.

radial profile of the electron density for cathode-directed streamers initiated with charge density distributions with $1/e$ diameters of 0.28 and 0.58 mm. In both cases, the diameter of the steady-state streamer body is a little larger than that of the initial ionization distribution, but the streamer from the distribution with the larger diameter continues to propagate with the larger diameter. Further, the ratio of the steady-state diameters of these two streamers as defined by the $1/e$ density points is about the same as the ratio of initial diameters.

Other properties of the streamers also depended on the diameter of the initial distribution. Figure 10 shows the electron density and axial electric field at a fixed time for cathode-directed streamers with initiating diameters of 0.28, 0.41, and 0.58 mm. The smaller diameter streamer produced a slightly higher field enhancement, and a shorter range for this enhancement than did the larger diameter streamer. Also, the density gradient at the tip was steeper and the propagation velocity was slower for the smaller diameter case. Similar behavior was observed for anode-directed streamers. Therefore, we conclude that at least for short gaps the dimensions of the initiating charge density play an important role in determining the characteristics of the propagating streamer. Whatever "forces" are in action to determine a natural streamer diameter must be weak.

C. Voltage dependence

To investigate the effect of applied field on streamer properties, we have carried out calculations with several applied voltages. We present the results of calculations with 18 kV applied across the 5-mm gap, giving an applied field of 36 kV/cm (134 Td) and corresponding to an overvoltage of about 2%. All other conditions were the same as for the calculations of Figs. 1 and 2, and the results are therefore directly comparable.

The time evolution of the electron density and axial electric field are shown in Fig. 11 for an anode-directed streamer with an applied voltage of 18 kV, corresponding to about 2% overvoltage. Here the velocity of the streamer ranges from about $3.6–5.0\times10^7$ cm/s, considerably slower than the $1–2\times10^8$ cm/s velocities found at 26 kV under otherwise identical conditions. These velocities are much larger than the electron drift velocity in the applied field (1.4×10^7 cm/s), and a little larger than the peak drift velocity at the tip ($2.5–3.2\times10^7$ cm/s). The ionization density in the tip and the peak field enhancements are about 50% and 20% smaller, respectively, than in the 26-kV case. The electron density gradient at the tip, on the other hand, is larger than in the 26-kV case, probably as a result of the much slower rate of electron impact ionization in the applied field ahead of the streamer.

The dependence of the cathode-directed streamer on voltage is different. At 18 kV the electron density reached extremely high values ($\approx10^{15}$ cm^{-3}). The initial propagation was slow, and the density gradient at the tip of the forming streamer became very steep, leading to numerical instabilities and forcing us to stop the calculation. At higher voltages, well-defined streamers were formed. The plasma density in the streamer body and the gradient of the electron density at the tip decreased with increasing field.

VI. NUMERICAL ACCURACY OF THE ALGORITHM

The flux corrector used in the FCT algorithm is strongly nonlinear, making estimates of the numerical error expected

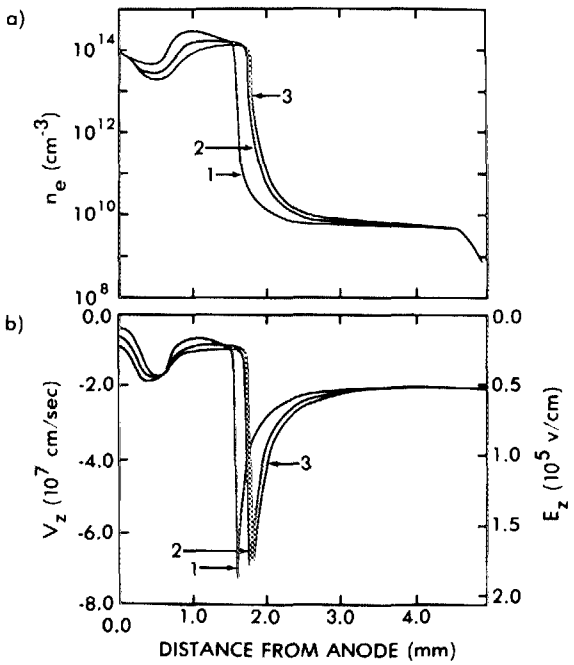

FIG. 10. Plots of (a) electron density and (b) axial electric field for cathode-directed streamers at $t = 2.0$ ns after the start of the simulation. All conditions were the same in Fig. 1, except that the $1/e$ diameter in the radial direction of the initiating plasma hemispheroid was (1) 0.28, (2) 0.41, and (3) 0.58 mm.

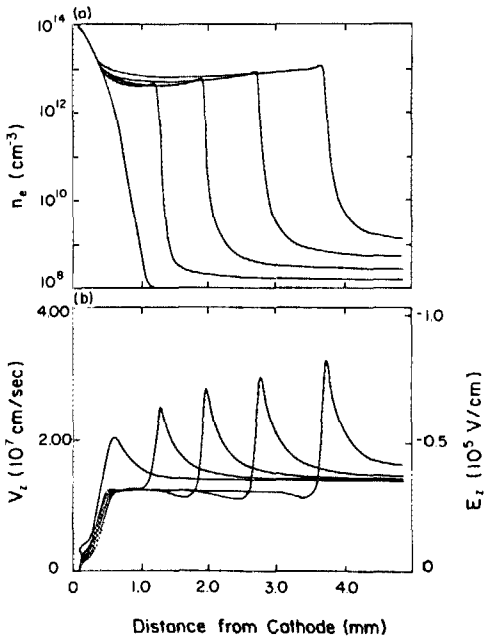

FIG. 11. Plots of (a) electron density and (b) axial electric field for an anode-directed streamer at $t = 0.2$, 2.0, 4.0, 6.0, and 8.0 ns after the start of the simulation. The charging voltage was 18 kV (134 Td), making the gap about 2% over-volted, and all other conditions are the same as in Fig. 2.

in any specific calculation difficult. Therefore, it is desirable to have an independent check on the accuracy of the algorithm. Such a check is provided by considering the velocity of a point of constant electron density. This quantity can be determined analytically from the continuity equations, Eqs. (1), in terms of quantities readily available from our calculation. The quantity can also be determined directly from the results of the calculation for the electron density for closely spaced times by simply noting how far a point of constant density moved during the time interval. Comparison of the two quantities provides a check on the numerical accuracy of the algorithm in solving Eqs. (1). An additional benefit of this analysis is that it provides insight into the relative importance of impact ionization, drift, and diffusion to streamer propagation.

We will use the term "phase velocity" to refer to the velocity of a point of constant electron density. To determine the phase velocity at the point $\mathbf{r}$ at time t_0, $\mathbf{v}_p(\mathbf{r},t_0)$, we seek a path, $\mathbb{P}(t)$ such that $\mathbb{P}(t_0)=\mathbf{r}$, and $(d/dt)n_e(\mathbf{P}(t),t)]_{t_0}=0$, or

$$\frac{\partial n_e(\mathbf{P},t)}{\partial t}+\frac{d\mathbf{P}}{dt}\cdot\nabla n_e(\mathbf{P},t)=0. \tag{14}$$

The quantity $d\mathbf{P}/dt$ is the desired phase velocity $\mathbf{v}_p$. On-axis we obtain from Eqs. (1) and (14), assuming $S=0$ in Eqs. (1),

$$v_p=\frac{dP_z}{dt}$$

$$=\left(-\alpha|v_e|+\nabla\cdot\mathbf{v}_e+\frac{D_L}{n_e}\frac{\partial^2 n_e}{\partial z^2}\right)\frac{\partial \ln n_e}{\partial z}+v_e. \tag{15}$$

The three terms in the numerator of Eq. (15) represent impact ionization, drift, and diffusion. Making use of Maxwell's first equation, we recognize the second term as the reciprocal of a sort of local dielectric relaxation time, $\nabla\cdot\mathbf{v}_e=\nabla\cdot\mu_e\mathbf{E}=\mu_e\rho/\epsilon_0$. Equation (15) can be extended to include other volume electron source and sink effects such as attachment, but probably cannot be modified to include a realistic model of photoionization. For ease of discussion we will refer to the value of v_p obtained by evaluating the right-hand side of Eq. (15) as the "indirect" value, and the value obtained directly from the output of the calculation as the "direct" value.

The results of applying Eq. (15) to the cathode-directed streamer shown in Figs. 1 and 5 at $t=1.0$ ns are shown in Fig. 12. The three curves show indirect phase velocities due to: (1) the dielectric relaxation term only, (2) the impact ionization term only, and (3) the complete expression for v_p. The contribution of the diffusion term was found to be negligible for nearly all calculations we have carried out. The discrete points plotted in Fig. 12 show the direct results obtained directly from the output of the program for the electron density at $t=1.0$ ns and $t=1.0\pm0.053$ ns. Throughout the region ahead of and in the streamer tip, the agreement is excellent. Behind the streamer tip the electron density is nearly constant in space, making the phase velocity poorly defined. In all but a few extreme cases we found similar agreement in calculations carried out for other conditions, indicating that the FCT algorithm was performing well. Note that the substitution of $\nabla\cdot\mathbf{v}_e$ with $\mu_e\rho/\epsilon_0$ brings the Poisson solver into the picture, so that the comparison of the two values for v_p then checks also on the accuracy with which Eq. (2) is solved.

Besides serving as a test of accuracy, the calculation of the phase velocity provides insight into the dynamics of

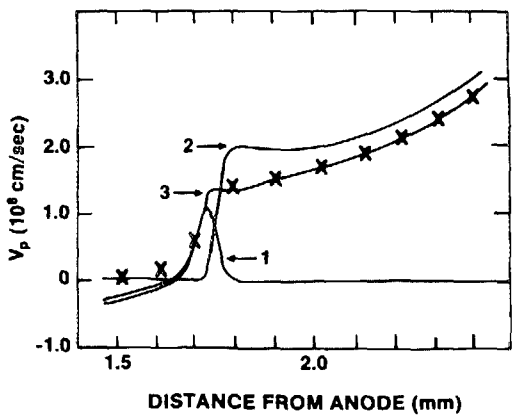

FIG. 12. Plot showing the phase velocity at $t=1.0$ ns after the start of the simulation for the cathode-directed streamer shown in Fig. 1. The solid lines show the indirect values and the x's show the direct values. The three solid curves correspond to (1) the dielectric relaxation contribution only, (2) the impact ionization contribution only, and (3) the complete expression for v_p in Eq. (12), i.e., the sum of (1) and (2) plus the diffusion term plus the drift velocity term.

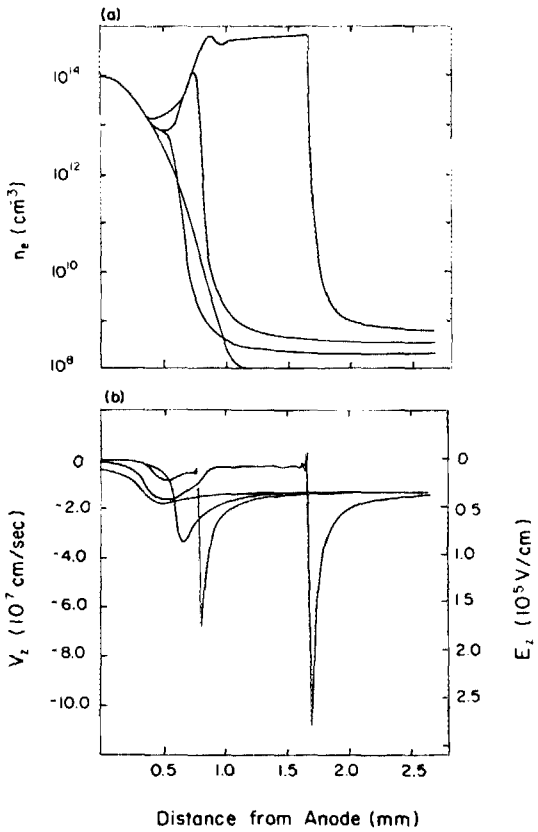

FIG. 13. Plots showing (a) electron density and (b) axial electric field for a cathode-directed streamer at 0.0, 2.0, 4.0, and 6.0 ns after the start of the simulation. The charging voltage was 18 kV (134 Td) and all other conditions were the same as in Fig. 1.

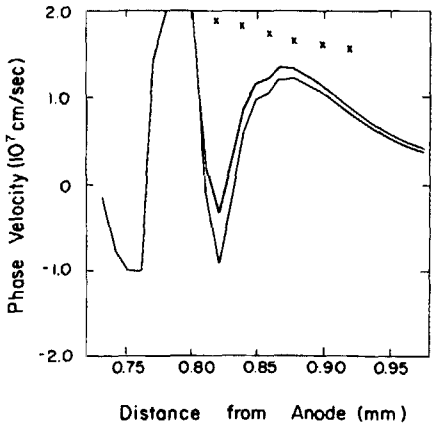

FIG. 14. Plot showing both indirect and direct phase velocities for the cathode-directed streamer shown in Fig. 13. The solid lines are "theoretical" results, with (1) showing the sum of the dielectric relaxation, impact ionization, and drift velocity terms, and (2) showing the effect of the addition of the diffusion term. The x's are the direct values.

streamer propagation. In a true steady-state propagation condition, the phase velocity would be constant, independent of position, and would correspond to the propagation velocity of the streamer. Variations of v_p with position determine the changes in shape of the streamer head with time. Furthermore, the separate calculation of the three terms contributing to v_p allows determination of the importance of the three processes to streamer propagation.

We have applied this analysis to the 18 kV (2% overvoltage) results for an anode-directed streamer shown in Fig. 11, and to the results of a similar calculation for a cathode-directed streamer, shown in Fig. 13. Inspecting the results for the electron density under these conditions, we see that the anode-directed streamer calculation seems well behaved, as does the cathode-directed streamer, except for the appearance of a small oscillation at 1.74 mm, which may be caused by the field calculator. Nevertheless, the slopes were quite steep, raising the possibility of numerical errors due to the eighth-order flux calculation algorithm being unable to follow such rapid variations.

Applying the error analysis discussed to our results for the anode-directed streamer showed that the algorithm was performing properly, but for the cathode-directed streamer these concerns proved justified, as can be seen in Fig. 14, which shows the phase velocity calculated from Eq. (12) along with the velocities obtained directly from the numerical results. The agreement is not good, implying numerical error. The reason for the error is probably a type of nonlinear numerical diffusion introduced by the flux calculator. It is not possible to fit an eighth-order polynomial to the nearly discontinuous change in n_e without severe overshoots between mesh points. The flux corrector then comes into play, removing the over-shoots, but introducing numerical diffusion caused by the first-order flux calculation scheme used in the limiter

It is interesting to note that in the cathode-directed case the density slope has become so steep that the diffusion term is no longer negligible, as demonstrated by the two curves in Fig. 14, which show the phase velocity calculated with and without the diffusion term in Eq. (12). Although not yet the dominant effect, the diffusion clearly is playing a role in the propagation. We experienced some difficulties modeling streamers at low applied voltages because of the steep electron density gradients encountered. This observation is encouraging for such studies because it implies that with only moderately increased spatial resolution it should be possible to model streamers at substantially lower voltage because diffusion will act to limit the electron density gradient at the streamer front.

VII. SUMMARY

We have studied in detail the formation and propagation of streamers. We used the flux-corrected transport algorithm to solve numerically the transport equations under strongly space-charge-dominated conditions such as occur at the head of a propagating streamer. The algorithm was fully two dimensional (three dimensional with cylindrical symmetry) and has proved stable and capable of dealing with the steep density gradients that appear in these calculations.

Under the conditions we have investigated we find:

(1) Once removed from the influence of the initial charge, the streamer reaches a quasi-steady state with typical velocities of $0.6–3.0\times10^8$ cm/s.

(2) For the conditions in our calculations we found the charge density in the body of the streamer to be about 10^{14} cm^{-3}, and to depend weakly on the ionization density ahead of the streamer and somewhat more strongly on the applied field. At low applied fields, there was a strong polarity dependence.

(3) The propagation velocity, ionization density in the main body, and the free-electron density ahead of a propagating streamer are related to each other once a quasi-steady state has been reached.

(4) The dielectric relaxation time is generally comparable to the time taken by the streamer to move the distance of the width of the shielding charge. As a result, the bulk of the plasma in the streamer is poorly shielded from the external field.

(5) The streamer characteristics in steady state are roughly independent of the magnitude of the density of the initiating ionization used to create the streamer.

(6) The diameter and other characteristics of the streamer are influenced by the diameter of the initial charge distribution.

(7) The propagation velocity and the streamer diameter increase with increasing applied field. For an anode-directed streamer, the ionization density and electron density gradient at the tip increase with increasing applied field, whereas for a cathode-directed streamer these quantities decrease.

(8) A simple expression for the velocity of a point of constant electron density exists. The expression is exact in the absence of a photoionization source term. Comparison of this result with the numerical results is useful in checking the accuracy of the numerical algorithm. The expression for the phase velocity divides into three physically identifiable terms: impact ionization term, a dielectric relaxation or shielding term, and a diffusion term. Comparison of the

magnitudes of each term provides insight into the dominant mechanism responsible for streamer behavior.

ACKNOWLEDGMENTS

The early stages of this work were supported by the U. S. Air Force Office of Scientific Research. We thank R. Morrow for originally pointing out the FCT algorithm to us, and the Texas Tech University Computing Center for providing computing time on a VAX 11/780 for many of the calculations reported here.

[1]H. Raether, Z. Phys. **112**, 464 (1939); Arch. Electrotech. **34**, 49 (1940).
[2]L. B. Loeb and J. M. Meek, J. Appl. Phys. **11**, 438 (1940).
[3]See for example J. Dutton, *Electrical Breakdown of Gases*, edited by J. M. Meek and J. D. Craggs (Wiley, New York, 1978), Chap. 3.
[4]J. K. Wright, Proc. R. Soc. London A **280**, 23 (1964).
[5]G. A. Dawson and W. P. Winn, Z. Phys. **183**, 159 (1965).
[6]D. L. Turcotte and R. S. B. Ong, J. Plasma Phys. **2**, 145 (1968).
[7]N. W. Albright and D. A. Tidman, Phys. Fluids **15**, 86 (1972).
[8]R. Klingbeil, D. A. Tidman, and R. F. Fernsler, Phys. Fluids **15**, 1969 (1972).
[9]A. J. Davies, C. S. Davies,and C. J. Evans, Proc. IEE **118**, 816 (1971).
[10]A. J. Davies, C. J. Evans, P. M. Townsend, and P. M. Woodison, Proc. IEE **124**, 179 (1977).
[11]L. E. Kline, J. Appl. Phys. **45**, 2046 (1974).
[12]K. Yoshida and H. Tagashira, J. Phys. D **9**, 491 (1976).
[13]A. J. Davies, C. J. Evans, and P. M. Woodison, Proc. IEE **12**, 765 (1975).
[14]K. Yoshida and H. Tagashira, J. Phys. D **9**, 485 (1976).
[15]E. Marode, J. Appl. Phys. **46**, 2016 (1975).
[16]I. Abbas and P. Bayle, J. Phys. D **13**, 1055 (1980).
[17]I. Abbas and P. Bayle, J. Phys. D **14**, 649 (1981).
[18]J. Dutton, J. Phys. Chem. Ref. Data **4**, 664 (1975).
[19]S. T. Zalesak, J. Comp. Phys. **31**, 335 (1979).
[20]J. P. Boris and D. L. Book, J. Comput. Phys. **11**, 39 (1973).
[21]See for examaple R. Morrow, Phys. Rev. A **32**, 1799 (1985).
[22]R. F. Fernsler, Ph. D. thesis, University of Maryland (1975).
[23]E. E. Kundhardt and C. Wu, J. Comput. Phys. **68**, 127 (1987).
[24]D. Potter, *Computational Physics* (Wiley, New York, 1977).
[25]E. E. Kunhardt and P. F. Williams, J. Comput. Phys. **57**, 403 (1985).
[26]See for example J. R. Reitz and F. J. Milford, *Foundations of Electromagnetic Theory* (Addison-Wesley, Reading, MA, 1960), p. 140.